Inital data for perturbed Kerr black holes on hyperboloidal slices

David Schinkel,[1] Marcus Ansorg,[1] and Rodrigo Panosso Macedo[1]

[1] *Theoretisch-Physikalisches Institut, Friedrich-Schiller-Universität Jena, Max-Wien-Platz 1, D-07743 Jena, Germany*

(Dated: January 30, 2013)

We construct initial data corresponding to a single perturbed Kerr black hole in vacuum. These data are defined on specific hyperboloidal slices on which the mean extrinsic curvature K asymptotically approaches a constant at future null infinity $\mathscr{I}^+$. More precisely, we require that K obeys the Taylor expansion $K = K_0 + \mathcal{O}(\sigma^4)$ where K_0 is a constant and σ describes a compactified spatial coordinate such that $\mathscr{I}^+$ is represented by $\sigma = 0$. We excise the singular interior of the black hole and assume a marginally outer trapped surface as inner boundary of the computational domain. The momentum and Hamiltonian constraints are solved by means of pseudo-spectral methods. We find exponential rates of convergence of our numerical solutions, and plan dynamical evolutions in a future project.

PACS numbers: 04.25.dg, 04.20.Ex

I. INTRODUCTION

One particular objective of numerical relativity is the study of gravitational waves emitted by the interaction of astrophysical objects. The corresponding wave forms permit the construction of templates for gravitational wave detections. Most of these calculations have been carried out on spatially truncated numerical domains. Despite their remarkable successes in recent years, the accuracy obtained was limited due to effects coming from artificial outer boundary conditions. Moreover, as the outgoing gravitational radiation is well-defined only at future null infinity $\mathscr{I}^+$, the wave extraction at finite distances causes additional inaccuracies.

An elegant alternative approach, which avoids these undesired effects, is the inclusion of $\mathscr{I}^+$ as outer boundary of the computational domain, i.e., the study of the spacetime on compactified hyperboloidal slices (see [1] for a review). This description permits the detailed analysis of the outgoing radiation through the Bondi news function [2, 3].

Note that, in this approach, the physical metric becomes singular at $\mathscr{I}^+$, which gives rise to a decomposition into a conformal factor, absorbing the singular behavior, and a regular *conformal* metric. Friedrich [4] has formulated a hyperbolic system for the conformal metric on hyperbolidal slices, which is equivalent to the Einstein equations. Unlike the Einstein equations, this system is manifestly regular at $\mathscr{I}^+$. The first numerical results of this system (in the context of weak relativistic fields were obtained) by Hübner [5].

Moncrief and Rinne [6] showed that the apparently singular boundary terms appearing in the hyperboloidal concept can be explicitly evaluated at $\mathscr{I}^+$ in terms of conformally regular geometric data. As a result of this analysis, they obtained a rather rigidly constrained and gauge fixed formulation of the field equations. The first stable dynamical numerical evolution based on this formulation was published by Rinne [7]. The corresponding code provides long-term stable and convergent evolutions of axisymmetrically perturbed Schwarzschild spacetimes.

The construction of initial data as a starting point for a subsequent dynamical evolution of the space time geometry requires the solution of coupled elliptic constraint equations, specifically the Hamiltonian and momentum constraints. In this paper we consider data which are defined on spatially compactified hyperboloidal slices extending up to $\mathscr{I}^+$. Previous calculations of such data have been carried out in the context of constant mean curvature (*"CMC-condition"*: K = constant throughout the slice). Important contributions were made by Frauendiener [8] and Buchman et al. [9]. While Frauendiener looked at slices with isotropic extrinsic curvature (that is, the extrinsic curvature is assumed to be proportional to the conformal 3-metric in the slice), Buchman et al. computed data in the context of conformal flatness, taking a generalization of the Bowen-York curvature [10] as the solution to the corresponding momentum constraint. In these cases, only the Hamiltonian constraint needs to be solved, and it is degenerate at $\mathscr{I}^+$ by virtue of the singular physical metric. For isotropic extrinsic curvature, the Hamiltonian constraint reduces to a form which is sometimes called the *Yamabe equation*. This equation has been studied extensively and solved numerically with pseudo-spectral methods by Frauendiener [8]. Andersson proved conditions under which the Yamabe equation has regular solutions [11]. These criteria were generalized by Andersson and Chruściel [12, 13] to the situation in which arbitrary slices obeying the CMC-condition are considered. As an example, these mathematical results apply to the slices used by Buchman et al. [9].

In this paper, we construct axially symmetric, conformally non-flat initial data corresponding to single perturbed Kerr black holes in vacuum on hyperboloidal slices. The corresponding constraint equations are considered in the conformal transverse traceless decomposition [14, 15]. In this formulation, the momentum constraint contains a term behaving like $\sigma^{-3}\nabla^i K$, where σ describes a compactified spatial coordinate such that $\mathscr{I}^+$ is represented by $\sigma = 0$. Now we can *regularize* the mo-

mentum constraint by requiring that the mean curvature K obeys the Taylor expansion $K = K_0+\mathcal{O}(\sigma^4)$ where K_0 is a constant. Henceforth, we call such slices *"ACMC"-slices*, as they fulfil the condition of *asymptotically constant mean curvature*. It turns out that the degenerate behavior of the corresponding Hamiltonian constraint is asymptotically the same as that of the Yamabe equation. For this reason, we call this behavior in the following *"Yamabe-like."*

As a starting point for our computations we take the Kerr solution in *Kerr coordinates* which are horizon-penetrating. Using the *"height-function"-technique* from Zenginoğlu [16], we apply a particular coordinate transformation in order to obtain compactified hyperboloidal ACMC-slices. This is to say, the coordinate transformation is chosen such that, in these compactified slices, the extrinsic mean curvature K is asymptotically constant, $K = K_0 + \mathcal{O}(\sigma^4)$. Now we consider the regular momentum constraint as well as the Yamabe-like Hamiltonian constraint that arises in the conformal transverse traceless approach. The corresponding computational domain is bounded by $\mathscr{I}^+$ (outer boundary) and by a marginally outer-trapped surface which serves as inner boundary. In other words, we excise the black hole interior and require that at the excision surface, the expansion of outgoing null rays vanishes. Of course, for the Kerr solution we started with, the constraints are identically satisfied. It is, however, easy to modify the set-up slightly and to compute initial data which correspond to *perturbed* Kerr black holes. To be more specific, we keep the coefficients, appearing in the constraint equations, as well as the boundary values of the solution to the momentum constraint as they are given by the Kerr solution in our ACMC-slices, but modify the *coordinate location* of the marginally outer-trapped surface. We then solve the constraints in the new computational domain given by the modified inner boundary and obtain perturbed Kerr black hole data. The deviation from the (unperturbed) Kerr solution is determined by a subsequent analysis. This analysis consists of the computation of mass and angular momentum multipoles that characterize the marginally outer-trapped surface. We find distinct differences with respect to the corresponding Kerr expressions which means that our numerical solutions cannot describe an unperturbed Kerr black hole.

The computation of these initial data has been realized by utilizing a single domain pseudo-spectral method which provides us with a rapid exponential convergence rate of the numerical solutions. This exponential fall-off is a strong indication that for the ACMC-slices the same regularity criteria hold as for strict CMC-slices.

The paper is organized as follows. In section II we construct hyperboloidal ACMC-slices of the Kerr solution. Next, in section III we discuss the constraint equations within the conformal transverse traceless decomposition and elaborate on regularity criteria valid at $\mathscr{I}^+$. The inner boundary is the subject of section IV, while we present the conditioning as well as the description of the numerical treatment is presented in section V. In section VI, we provide exemplary results corresponding to strongly perturbed Kerr data as well as to weakly perturbed data with large rotation parameter. We conclude in section VII with a discussion and a perspective of future work. The appendix contains the explicit form of the auxiliary function A used in the coordinate transformation to obtain ACMC-slices (see section VIII A), a comparison between CMC- and ACMC-slices in the Schwarzschild case (see VIII B) and, finally, section VIII C in which the multipole analysis of the constructed data is described.

Note that we use the following conventions. Greek indices run from 0 to 3 where 0 denotes the time component. Small latin indices are from 1 to 3, covering spatial indices. Conformal (unphysical) objects will be decorated with a tilde. We use units in which the speed of light as well as Newton's constant of gravitation are unity.

II. THE KERR SOLUTION IN ACMC SLICES

As mentioned above, the construction of initial data pursued in this paper is based on the conformal transverse traceless decomposition of the constraints on compactified hyperboloidal slices. In order to regularize the momentum constraint in this formulation, we consider ACMC-slices on which the mean curvature K obeys the Taylor expansion $K = K_0 + \mathcal{O}(\sigma^4)$. In the following, we identify such slices within the Kerr solution, which then will serve as a starting point for the generation of perturbed Kerr data.

We begin with the horizon-penetrating line element in Kerr coordinates (V, r, θ, φ),

$$\begin{aligned} ds^2 = &-\left(1-\frac{2Mr}{\rho^2}\right)dV^2 + 2dVdr \\ &- \frac{4Mra}{\rho^2}\sin^2\theta\, dVd\varphi + \rho^2 d\theta^2 - 2a\sin^2\theta\, drd\varphi \\ &+ \frac{1}{\rho^2}\left[\left(r^2+a^2\right)^2 - \Delta a^2\sin^2\theta\right]\sin^2\theta\, d\varphi^2. \end{aligned} \quad (1)$$

Here we have

$$\rho = \sqrt{r^2 + a^2\cos^2\theta}, \qquad \Delta = r^2 - 2Mr + a^2, \quad (2)$$

where M and $J = aM$ are, respectively, the mass and angular momentum of the black hole. Note that in the following we use the dimensionless angular momentum parameter

$$j = \frac{a}{M} = \frac{J}{M^2}.$$

The event horizon of the black hole is located at $r = r_{\mathrm{h}} = M(1+\sqrt{1-j^2})$ which runs from $r_{\mathrm{h}} = 2M$ in the Schwarzschild case ($j = 0$) to $r_{\mathrm{h}} = M$ for the extreme Kerr black hole ($|j| = 1$).

We introduce hyperboloidal slices through a coordinate transformation that is motivated by an asymptotic integration of outgoing radial null rays, defined by

$$ds^2 = 0, \quad d\theta = 0, \quad d\varphi = 0, \quad dV dr > 0.$$

The corresponding equation

$$dV = \frac{2dr}{1 - \dfrac{2Mr}{\rho^2}} = 2\left[1 + \frac{2M}{r} + \mathcal{O}(r^{-2}\right] dr \tag{3}$$

is solved asymptotically by

$$V = 4M\left[\text{constant} + \left(\frac{r}{2M} + \log\frac{r}{2M}\right)\right].$$

From this form, we obtain a coordinate transformation which leads us from Kerr coordinates to general axially symmetric, compactified hyperboloidal slices by the *ansatz*[1]

$$r = \frac{2M}{\sigma} \tag{4}$$

$$V = 4M\left[\tau + \underbrace{\left(\frac{1}{\sigma} - \log(\sigma) + A(\sigma, \cos\theta)\right)}_{h}\right]. \tag{5}$$

In the new coordinates $(\tau, \sigma, \theta, \varphi)$, the compactified hyperboloidal slices are described by $\tau =$ constant. The coordinate location of future null infinity $\mathscr{I}^+$ is given by $\sigma = 0$ while the event horizon is placed at

$$\sigma = \sigma_{\rm h} = \frac{2}{1 + \sqrt{1 - j^2}}. \tag{6}$$

The coefficients $g_{\mu\nu}$ of the physical metric can be written in the form

$$g_{\mu\nu} = \Omega^{-2}\tilde{g}_{\mu\nu}. \tag{7}$$

Here, $\tilde{g}_{\mu\nu}$ denotes a conformal metric, which is regular everywhere, and Ω is a *conformal factor* that vanishes linearly at $\mathscr{I}^+$, i.e. $\Omega|_{\mathscr{I}^+} = 0$, $\partial_\sigma\Omega|_{\mathscr{I}^+} \neq 0$. For the function A appearing in (5), an arbitrary regular expression in terms of σ and

$$\mu := \cos\theta \in [-1, 1]$$

can be chosen[2], as long as one ensures that the resulting hyperboloidal slices $\tau =$ constant are spacelike everywhere away from $\mathscr{I}^+$. This construction of hyperboloidal slices is equivalent to the *height function technique* [16], and the corresponding height function h is indicated in (5).

In the following we make use of the freedom to choose the regular function A in order to generate slices that satisfy the ACMC-condition

$$K = K_0 + \mathcal{O}(\sigma^4), \qquad K_0 = \text{constant}. \tag{8}$$

Here K is the *mean curvature*

$$K = K_{\mu\nu}g^{\mu\nu}, \tag{9}$$

i.e., the trace of the *extrinsic curvature* $K_{\mu\nu}$,

$$K_{\mu\nu} = \frac{1}{2}\mathcal{L}_n g_{\mu\nu}. \tag{10}$$

In this definition, $\mathcal{L}_n$ is the Lie derivative along the future pointing unit vector n^μ normal to the slices $\tau =$ constant. We follow the sign convention employed by Wald [17], which was also used in [9]. In this convention (opposite to the widely adopted one by Misner, Thorne & Wheeler [18]), the mean curvature K assumes *positive* values at $\mathscr{I}^+$.

Now, for a given function $A(\sigma, \mu)$, the Taylor expansion of K with respect to σ at $\mathscr{I}^+$ ($\sigma = 0$), considered in a slice $\tau =$ constant, has the following structure:

$$K = K_0 + K_1\sigma^1 + K_2\sigma^2 + K_3\sigma^3 + O(\sigma^4) \tag{11}$$

with rather longish expressions for the coefficients $K_j = K_j(\mu)$. Putting $K_0 =$ constant and $K_1 = K_2 = K_3 \equiv 0$, we obtain asymptotic conditions for $A(\sigma, \mu)$,

$$A\Big|_{\sigma=0} = a_0 \tag{12}$$

$$\partial_\sigma A\Big|_{\sigma=0} = a_1 - \frac{j^2\mu^2}{16} \tag{13}$$

$$\partial_\sigma^2 A\Big|_{\sigma=0} = -1 + \frac{j^2}{4} \tag{14}$$

$$\partial_\sigma^3 A\Big|_{\sigma=0} = -2(4 + 6a_1 + 3a_1^2) + j^2\left(1 + \frac{3}{4}\mu^2(1 + a_1) - \frac{3}{128}j^2\mu^4\right), \tag{15}$$

with a_0 and a_1 being arbitrary, unconstrained constants.

As mentioned above, we need to ensure that the corresponding slices $\tau =$ constant are spacelike, which means that the conformal lapse

$$\tilde{\alpha} = \Omega\alpha = \frac{1}{\sqrt{-\tilde{g}^{00}}}$$

is well defined everywhere. Now, for numerical reasons, it would be desirable to have a "very" smooth function $\tilde{\alpha}$, meaning that a spectral expansion with respect to Chebyshev polynomials shows a rapid exponential fall-off of the corresponding coefficients $\left|c_k^{(\tilde{\alpha})}\right|$[3]. Indeed we find

[1] Note that through this ansatz we retain the horizon penetrating nature of the coordinates.

[2] The requirement of axisymmetry implies that A has to depend on $\cos\theta$, which we denote henceforth by μ.

[3] As a representative, we consider $\tilde{\alpha}(\sigma, \mu = 0)$, i.e. the conformal lapse as a function of $\sigma \in [0, \sigma_{\rm h}]$ along the equatorial plane $\theta = \pi/2$.

that a rapid convergence rate of these coefficients is a good indication of high numerical accuracy of the results obtained from the subsequent pseudo-spectral solution of the constraints. We thus aim at a choice for the function A such that on the one hand the conditions (12)-(15) are satisfied and on the other hand the $|c_k^{(\tilde{\alpha})}|$ fall off rapidly.

We have found that these requirements are met by an appropriate diagonal Padé expansion. In this approach, the coefficients $b_k = b_k(\mu)$ and $c_k = c_k(\mu)$ of the rational function

$$\mathfrak{P}_n(\sigma,\mu) = \frac{\sum_{k=0}^{n} b_k \sigma^k}{1 + \sum_{k=1}^{n} c_k \sigma^k} \tag{16}$$

are determined by the first $2n$ derivatives of A at $\sigma = 0$, i.e. through the conditions given in (12)-(15). Since a_0 represents an irrelevant time shift, we can set it to zero, which implies $b_0 = 0$. In order to satisfy the remaining three conditions (13)-(15), we need at least a second order Padé expansion, $n = 2$, which provides us with the freedom to choose a parameter, say a_4, describing the fourth derivative $\partial_\sigma^4 A\Big|_{\sigma=0}$. In this way, our Padé approximation contains two undetermined parameters, a_1 and a_4, and we can use this freedom in order to obtain rapid fall-off rates of the corresponding spectral coefficients $c_k^{(\tilde{\alpha})}$. A satisfactory choice is given by

$$a_1 = \frac{113}{100} + \frac{9}{500}|j| + \frac{3}{40}j^2 \tag{17}$$

$$a_4 = 4!\,\left(\frac{161}{10} + \frac{3}{4}|j| - \frac{5}{2}j^2\right), \tag{18}$$

which describes the two constants parametrically in terms of the dimensionless angular momentum j. The explicit form of the resulting function

$$A(\sigma,\mu) = \mathfrak{P}_2(\sigma,\mu) \tag{19}$$

as well as a discussion regarding the derivation of the choice (17,18) can be found in Appendix VIII A. Note that the corresponding mean curvature K assumes the required ACMC-structure,

$$K(\sigma,\mu) = \frac{3}{M\sqrt{16(1+a_1) - j^2}} + O(\sigma^4). \tag{20}$$

III. THE CONSTRAINTS IN THE CONFORMAL TRANSVERSE TRACELESS DECOMPOSITION ON COMPACTIFIED HYPERBOLOIDAL ACMC-SLICES

A. Constraint equations

In the standard 3+1 decomposition of spacetime, the line element is written as

$$ds^2 = -\alpha^2 dt^2 + \gamma_{ij}\left(dx^i + \beta^i dt\right)\left(dx^j + \beta^j dt\right). \tag{21}$$

with α being the *lapse* function, β^i the *shift vector*, and γ_{ij} the induced three-metric of the spatial slice. The constraint equations valid in that slice are the momentum constraints

$$\nabla_i(K^{ij} - \gamma^{ij}K) = 0 \tag{22}$$

and the Hamiltonian constraint

$$R + K^2 - K_{ij}K^{ij} = 0. \tag{23}$$

Here, ∇_i is the covariant derivative associated with the induced metric γ_{ij}, and R is the associated curvature scalar, while the K_{ij} denote the spatial components of the extrinsic curvature.

There are several formulations for decomposing the constraint equations. Here we use the *conformal transverse traceless decomposition* (CTT) [14, 15], in which we write

$$\begin{aligned} K_{ij} &= \Omega\tilde{A}_{ij} + \frac{1}{3\Omega^2}\tilde{\gamma}_{ij}K, \\ K^{ij} &= \Omega^5\tilde{A}^{ij} + \frac{\Omega^2}{3}\tilde{\gamma}^{ij}K \end{aligned} \tag{24}$$

with the conformal three-metric defined as

$$\tilde{\gamma}_{ij} = \Omega^2\gamma_{ij}, \qquad \tilde{\gamma}^{ij} = \Omega^{-2}\gamma^{ij},$$

and the traceless part $\tilde{A}^{ij}$,

$$\tilde{\gamma}_{ij}\tilde{A}^{ij} = 0 = \tilde{\gamma}^{ij}\tilde{A}_{ij}.$$

We further decompose $\tilde{A}^{ij}$ as

$$\tilde{A}^{ij} = (\tilde{\mathcal{L}}V)^{ij} + M^{ij}, \tag{25}$$

where

$$(\tilde{\mathcal{L}}V)^{ij} = \tilde{\nabla}^i V^j + \tilde{\nabla}^j V^i - \frac{2}{3}\tilde{\gamma}^{ij}\tilde{\nabla}_k V^k$$

and $\tilde{\nabla}_i$ denotes the covariant derivative with respect to $\tilde{\gamma}_{ij}$.

In the CTT approach, the symmetric tracefree tensor M^{ij}, the mean curvature K, and the conformal metric $\tilde{\gamma}_{ij}$ are considered as freely specifiable data. Given these, the momentum constraint becomes

$$\tilde{\Delta}_{\mathcal{L}}V^i = \frac{2}{3\Omega^3}\tilde{\nabla}^i K - \tilde{\nabla}_j M^{ij} \tag{26}$$

with

$$\tilde{\Delta}_{\mathcal{L}}V^i = \tilde{\nabla}_j(\tilde{\mathcal{L}}V)^{ij}.$$

To rewrite the Hamiltonian constraint, we use the decomposition (see, e.g., [1])

$$\Omega = \omega\phi^{-2}, \tag{27}$$

where ω is a prescribed spatial function[4] which describes $\mathscr{I}^+$ by $\omega|_{\mathscr{I}^+}=0$. Note that ω has similar properties to Ω, i.e., it is positive away from $\mathscr{I}^+$ and possesses non-vanishing gradient at $\mathscr{I}^+$. The auxiliary potential ϕ is chosen to be positive everywhere.

The Hamiltonian constraint then turns into

$$-\left(\omega^2\tilde{R}+4\omega\tilde{\nabla}^2\omega-6\tilde{\nabla}^a\omega\tilde{\nabla}_a\omega\right)\phi-8\omega\tilde{\nabla}^a\phi\tilde{\nabla}_a\omega +8\omega^2\tilde{\nabla}^2\phi=\frac{2}{3}K^2\phi^5-\omega^6\tilde{A}_{ij}\tilde{A}^{ij}\phi^{-7}. \quad (28)$$

Here $\tilde{R}$ denotes the curvature scalar associated with $\tilde{\gamma}_{ij}$. Note that for isotropic extrinsic curvature, $\tilde{A}_{ij}\equiv 0$, the last term vanishes, and (28) turns into the *Yamabe equation*[5].

Finally, with the decomposition of the conformal factor (27), the momentum constraints read as

$$\tilde{\Delta}_{\mathcal{L}}V^i=\frac{2}{3}\frac{\phi^6}{\omega^3}\tilde{\nabla}^iK-\tilde{\nabla}_jM^{ij}. \quad (29)$$

In sum, the determination of valid initial data on compactified hyperboloidal slices in the CTT approach consists of the solution of the conformal constraint system (28, 29) for the potentials ϕ and V^i. As mentioned above, M^{ij}, K,$\tilde{\gamma}_{ij}$ as well as ω are prescribed quantities, and $\tilde{A}^{ij}$ is given in terms of V^i and M^{ij} by equation (25).

B. Regularity of the constraint equations

The momentum constraint (29) contains a term $\sim\Omega^{-3}\tilde{\nabla}^iK$ which is regular up to $\mathscr{I}^+$ only when the mean curvature satisfies the ACMC-condition

$$K=K_0+K_4\omega^4, \qquad K_0=\text{constant}. \quad (30)$$

If the global CMC condition is imposed, that is $K_4\equiv 0$, then the constraints decouple, i.e., at first, the momentum constraints can be solved for V^i and then the Hamiltonian constraint for ϕ. Although we lose this separability for $K_4\not\equiv 0$, we retain the structure of the constraint equations at $\mathscr{I}^+$. To be more specific, the momentum constraint is a completely regular elliptic system of differential equations, requiring the prescription of inner and outer boundary conditions for a unique solution. At the same time, the Hamiltonian constraint assumes a *Yamabe-like* structure, i.e. it looks asymptotically up to order ω^4 like the *Yamabe equation*. As a consequence, the first three terms ϕ_0,ϕ_1,ϕ_2 of a Taylor expansion of ϕ, taken in normal direction with respect to $\mathscr{I}^+$, can be found explicitly,

$$\phi=\phi_0+\phi_1\omega+\phi_2\omega^2+\text{higher order terms}, \quad (31)$$

e.g., for ϕ_0 we obtain:

$$\phi_0=\sqrt[4]{9K_0^{-2}(\tilde{\nabla}^a\omega\tilde{\nabla}_a\omega)|_{\mathscr{I}^+}}. \quad (32)$$

All terms higher than quadratic order cannot be determined *a priori*, but follow from the global solution of the constraint system if boundary conditions are imposed.

Andersson and Chruściel investigated regularity criteria valid for solutions to the Hamiltonian constraint on hyperboloidal slices satisfying the CMC-condition [11, 12]. They found that ϕ (and hence Ω) is analytic in a vicinity of $\mathscr{I}^+$ provided that at $\mathscr{I}^+$, the conformal extrinsic curvature

$$\tilde{\kappa}_{ij}=\frac{1}{2}\mathcal{L}_{\tilde{s}}\tilde{q}_{ij} \quad (33)$$

is proportional to the induced conformal metric

$$\tilde{q}_{ij}=\tilde{\gamma}_{ij}-\tilde{s}_i\tilde{s}_j, \quad (34)$$

that is, that there is a scalar λ defined on $\mathscr{I}^+$ such that

$$(\tilde{\kappa}_{ij}-\lambda\tilde{q}_{ij})\,|_{\mathscr{I}^+}=0. \quad (35)$$

Here, $\tilde{s}^i$ is the conformal unit vector normal to $\mathscr{I}^+$ in the hyperboloidal slice. The condition (35) is equivalent to requiring that $\mathscr{I}^+$ be *shear-free*.

In this work we assume that the shear-freeness of $\mathscr{I}^+$ (35) ensures likewise the regularity of solutions to the constraint system (28, 29) which arise in the context of the more general ACMC-condition. As we use for the conformal metric $\tilde{\gamma}_{ij}$ the Kerr expression in ACMC-slices (constructed in section II), we can explicitly check the validity of (35). We find $\lambda\equiv 0$, i.e., the condition is fulfilled in a trivial manner.

Note that for CMC slice in general, the Taylor expansion of the auxiliary potential ϕ, taken in the normal direction with respect to $\mathscr{I}^+$, breaks down at 3rd order in ω, i.e. ,terms $\propto\omega^3\log(\omega)$ appear. These logarithmic terms vanish if the shear-freeness of $\mathscr{I}^+$ [i.e., Eq. (35)] is imposed. Bardeen et al. [19] discuss the fact that this condition is equivalent to the absence of outgoing radiation at $\mathscr{I}^+$. Here we are interested in completely regular initial data which do not possess these logarithmic terms. Following the arguments presented in [19], we conclude that the data constructed below do not carry outgoing radiation.

IV. MARGINALLY OUTER-TRAPPED SURFACES AS INNER BOUNDARIES

In this paper, we compute initial data corresponding to a perturbed Kerr black hole in vacuum. In order to describe the black hole, we excise its singular interior and require the excision boundary $\mathcal{H}$ to be a marginally outer-trapped surface [20]. We thus obtain an inner boundary of our computational domain.

[4] In this paper, we choose ω to always agree with the compactified radial coordinate σ.

[5] Isotropic extrinsic curvature implies $K=$ constant, i.e., the corresponding slices satisfy the CMC-condition.

For a marginally outer-trapped surface, the expansion scalar of the 2-manifold embedded into the 3-slices vanishes for outgoing null rays. The corresponding condition reads

$$\nabla_a s^a + K - s^a s^b K_{ab} = 0, \tag{36}$$

where s^a is the outward pointing unit vector normal to the surface $\mathcal{H}$ in the 3-slice.

Note that in ACMC-slices of the Kerr solution (see section II), this condition is satisfied at the location of the event horizon $r = r_{\rm h}$, corresponding to $\sigma = \sigma_{\rm h} = 2/(1+\sqrt{1-j^2})$. Furthermore, this surface is the *outermost* marginally trapped surface, i.e., the *apparent horizon* [21].

Writing (36) in terms of conformal quantities, we get an inner boundary condition valid at $\mathcal{H}$, containing ϕ as well as its first derivatives,

$$\tilde{s}^a\partial_a\phi + \frac{\phi}{4}\left(\tilde{\nabla}_a\tilde{s}^a - \frac{2\tilde{s}^a\partial_a\omega}{\omega}\right) + \frac{K\phi^3}{6\omega} - \frac{\omega^2}{4\phi^3}\tilde{s}^a\tilde{s}^b\tilde{A}_{ab} = 0. \tag{37}$$

Here we used the equations (7, 24 and 27) and introduced the conformal normal vector $\tilde{s}^i = \Omega^{-1}s^i$.

For the construction of perturbed Kerr data below, we require this condition at a coordinate location $\sigma_{\mathcal{H}}$ that differs from the Kerr value $\sigma_{\rm h}$ [see Eq. (6)]. At the same time, we keep all coefficients in the constraint equations as well as the boundary conditions of the vector V^i in the form that results from the Kerr solution in ACMC slices. If the perturbation is chosen to be sufficiently small, we ensure that the corresponding marginally outer-trapped surface will be outermost [22, 23], i.e., the apparent horizon[6].

V. NUMERICAL SOLUTION OF THE CONSTRAINT EQUATIONS

In this section we explicitly describe the steps in the set-up of the constraints and their numerical solution. Using the coordinates $(x^0, x^1, x^2, x^3) = (\tau, \sigma, \mu, \varphi)$ and putting $\omega = \sigma$, we write the Hamiltonian constraint as

$$H_1\phi_{,11} + H_2\phi_{,22} + H_3\phi_{,12} + H_4\phi_{,1} + H_5\phi_{,2} + H_6\phi + H_7\phi^5 + H_8\phi^{-7} = 0, \tag{38}$$

where the H_j are defined as:

$$\begin{aligned}
H_1 &= 8\sigma^2\tilde{\gamma}^{11}\\
H_2 &= 8\sigma^2\tilde{\gamma}^{22}\\
H_3 &= 16\sigma^2\tilde{\gamma}^{12}\\
H_4 &= -8\sigma^2\tilde{\gamma}^{ab}\tilde{\Gamma}^1_{ab} - 8\sigma\tilde{\gamma}^{11}\\
H_5 &= -8\sigma^2\tilde{\gamma}^{ab}\tilde{\Gamma}^2_{ab} - 8\sigma\tilde{\gamma}^{2\,1}\\
H_6 &= -\sigma^2\tilde{R} + 4\sigma\tilde{\gamma}^{ab}\tilde{\Gamma}^1_{ab} + 6\tilde{\gamma}^{11}\\
H_7 &= -\frac{2}{3}K^2\\
H_8 &= \sigma^6(\mathfrak{k}^{ij\,b}{}_a V^a{}_{,b} + \mathfrak{l}^{ij}{}_a V^a + \mathfrak{m}^{ij})\\
&\quad\times(\mathfrak{k}_{ij}{}^b{}_a V^a{}_{,b} + \mathfrak{l}_{ija}V^a + \mathfrak{m}_{ij}).
\end{aligned} \tag{39}$$

By virtue of the decomposition (25) we have written here $\tilde{A}^{ij}$ and $\tilde{A}_{ij}$ as

$$\begin{aligned}
\tilde{A}^{ij} &= \mathfrak{k}^{ijb}{}_a V^a{}_{,b} + \mathfrak{l}^{ij}{}_a V^a + \mathfrak{m}^{ij}\\
\tilde{A}_{ij} &= \mathfrak{k}_{ij}{}^b{}_a V^a{}_{,b} + \mathfrak{l}_{ija}V^a + \mathfrak{m}_{ij},
\end{aligned} \tag{40}$$

where $\mathfrak{k}$, $\mathfrak{l}$, $\mathfrak{m}$ are given by

$$\begin{aligned}
\mathfrak{k}^{ijb}{}_a &= \tilde{\gamma}^{bi}\delta^j_a + \tilde{\gamma}^{bj}\delta^i_a - \frac{2}{3}\tilde{\gamma}^{ij}\delta^b_a\\
\mathfrak{l}^{ij}{}_a &= \left(\tilde{\gamma}^{ki}\tilde{\Gamma}^j_{ka} + \tilde{\gamma}^{kj}\tilde{\Gamma}^j_{ka} - \frac{2}{3}\tilde{\gamma}^{ij}\tilde{\Gamma}^k_{ka}\right)\\
\mathfrak{m}^{ij} &= M^{ij}
\end{aligned} \tag{41}$$

and

$$\begin{aligned}
\mathfrak{k}_{ij}{}^b{}_a &= \tilde{\gamma}_{aj}\delta^b_i + \tilde{\gamma}_{ia}\delta^b_j - \frac{2}{3}\tilde{\gamma}_{ij}\delta^b_a\\
\mathfrak{l}_{ija} &= \left(\tilde{\gamma}_{kj}\tilde{\Gamma}^k_{ia} + \tilde{\gamma}_{ik}\tilde{\Gamma}^k_{ja} - \frac{2}{3}\tilde{\gamma}_{ij}\tilde{\Gamma}^k_{ka}\right)\\
\mathfrak{m}_{ij} &= M_{ij}.
\end{aligned} \tag{42}$$

The momentum constraints read

$$\mathfrak{a}^{irq}{}_p V^p{}_{,qr} + \mathfrak{b}^{iq}{}_p V^p{}_{,q} + \mathfrak{c}^i{}_p V^p + \mathfrak{d}^i + \mathfrak{e}^i\phi^6 = 0, \tag{43}$$

where

$$\begin{aligned}
\mathfrak{a}^{irq}{}_p &= \tilde{\gamma}^{qr}\delta^i_p + \frac{1}{6}\left(\tilde{\gamma}^{ir}\delta^q_p + \tilde{\gamma}^{iq}\delta^r_p\right)\\
\mathfrak{b}^{iq}{}_p &= \tilde{\gamma}^{i\,q}\tilde{\Gamma}^j{}_{j\,p} - \tilde{\gamma}^{j\,k}\tilde{\Gamma}^q{}_{j\,k}\delta^i_p + \tilde{\gamma}^{j\,q}\tilde{\Gamma}^i{}_{j\,p} + \tilde{\gamma}^{q\,k}\tilde{\Gamma}^i{}_{k\,p}\\
&\quad -\frac{2}{3}\tilde{\gamma}^{i\,q}\tilde{\Gamma}^k{}_{k\,p}\\
\mathfrak{c}^i{}_p &= \tilde{\gamma}^{ik}\left(\tilde{\Gamma}^j_{kp,j} - \tilde{\Gamma}^l_{jk}\tilde{\Gamma}^j_{lp} + \tilde{\Gamma}^j_{jl}\tilde{\Gamma}^l_{kp}\right)\\
&\quad +\tilde{\gamma}^{jk}\left(\tilde{\Gamma}^i_{kp,j} - \tilde{\Gamma}^l_{jk}\tilde{\Gamma}^i_{lp} + \tilde{\Gamma}^i_{jl}\tilde{\Gamma}^l_{kp}\right)\\
&\quad -\frac{2}{3}\tilde{\gamma}^{ij}\left(\tilde{\Gamma}^k_{kp,j} - \tilde{\Gamma}^l_{jk}\tilde{\Gamma}^k_{lp} + \tilde{\Gamma}^k_{jl}\tilde{\Gamma}^l_{kp}\right)\\
\mathfrak{d}^i &= \tilde{\nabla}_j M^{ij}\\
\mathfrak{e}^i &= -\frac{2}{3\sigma^3}\tilde{\gamma}^{ij}\partial_j K.
\end{aligned} \tag{44}$$

In order to derive particular numerical values for this set of conformal coefficients, we first need to specify the

[6] Even though stronger perturbations may lead to solutions for which the apparent horizon could be located further out [24], supplementary investigations of the computed solutions strongly indicate that, in these cases, we are also dealing with the apparent horizon (see appendix VIII C).

conformal factor $\Omega_{\rm Kerr}$ that we take for the conformal decomposition of the unperturbed Kerr metric in ACMC slices. We put

$$\Omega_{\rm Kerr} = \frac{\sigma}{4M},$$

leading via (27) with $\omega = \sigma$ to $\phi_{\rm Kerr} \equiv 2\sqrt{M}$. Then all coefficients denoted in Fraktur letters as well as $\{H_1, \ldots, H_7\}$ follow explicitly from the Kerr solution in ACMC slices. In particular, the quantities $\mathfrak{e}^i$ are regular at $\mathscr{I}^+$ by virtue of the ACMC condition [cf. equation (20)]. The coefficients $\mathfrak{m}^{ij}$ are obtained by requiring that the unperturbed Kerr solution satisfies the momentum constraints through $V^i_{\rm Kerr} \equiv 0$. Using (25), we conclude that

$$\mathfrak{m}^{ij} = \tilde{A}^{ij}_{\rm Kerr}.$$

Now, for solving the constraints uniquely, we still need to impose boundary conditions. As the momentum constraints are a completely regular, non-degenerate system of elliptic equations, we may simply choose trivial Dirichlet boundary conditions for the potentials V^i,

$$V^i\Big|_{\mathscr{I}^+} = 0 = V^i\Big|_{\mathcal{H}}. \tag{45}$$

Note that other choices are possible. Indeed any condition that is compatible with $V^i_{\rm Kerr} \equiv 0$ in the unperturbed case will do. In contrast, the potential ϕ is not subject to freely specifiable boundary conditions. On the one hand, the Yamabe-like Hamiltonian constraint provides us with a regularity condition valid at $\mathscr{I}^+$,

$$\phi\Big|_{\mathscr{I}^+} = \left[\sqrt[4]{9\tilde{\gamma}^{11}K^{-2}}\right]_{\mathscr{I}^+}, \tag{46}$$

which is equivalent to (32). On the other hand, we require our inner boundary $\mathcal{H}$ to be a marginally outer trapped surface, which means that (37) yields the boundary condition

$$\left[\tilde{s}^a\partial_a\phi + \mathfrak{h}_1\phi + \mathfrak{h}_2\phi^3 + \mathfrak{h}_3\phi^{-3}\right]_{\mathcal{H}} = 0 \tag{47}$$

where the $\mathfrak{h}_i$ are defined through

$$\begin{aligned}
\mathfrak{h}_1 &= \frac{1}{4}\left(\tilde{\nabla}_a\tilde{s}^a - \frac{2}{\sigma}\tilde{s}^1\right)\\
\mathfrak{h}_2 &= \frac{K}{6\sigma}\\
\mathfrak{h}_3 &= -\frac{\sigma^2}{4}\tilde{s}^a\tilde{s}^b\tilde{A}_{ab}.
\end{aligned} \tag{48}$$

As already mentioned, we impose this condition at $\sigma = \sigma_{\mathcal{H}} \neq \sigma_{\rm h}$ [see Eq. (6)], in order to obtain *perturbed* Kerr data. This is the only perturbation we perform, though various other choices are possible. We solve the coupled elliptic system (38, 43) together with the boundary conditions (45, 46, 47) by means of a single-domain pseudo-spectral Gauss-Lobatto method. For prescribed numerical resolutions N_σ and N_μ, the collocation points are given through

$$\begin{aligned}
\sigma_j &= \sigma_{\mathcal{H}}\sin^2\left(\frac{\pi j}{2N_\sigma}\right) \quad (j = 0, \ldots, N_\sigma)\\
\mu_k &= -\cos\left(\frac{\pi k}{N_\mu}\right) \qquad (k = 0, \ldots, N_\mu),
\end{aligned} \tag{49}$$

which are the abscissa values of the local extrema of the Chebyshev polynomials $T_{N_\sigma}(2\sigma/\sigma_{\mathcal{H}} - 1)$ and $T_{N_\mu}(\mu)$ respectively[7]. As described in detail e.g., in [25], the values $(\phi_{jk}, V^1_{jk}, V^2_{jk}, V^3_{jk})$ of the unknown potentials at these collocation points are combined to form a vector $\mathbf{f}^{(N_\sigma, N_\mu)}$. From any such vector, the Chebyshev coefficients of the potentials as well as those of their first and second derivatives can be computed. The combination of constraints and boundary conditions, evaluated at the points (49), yields a non-linear system of algebraic equations of order $4 \times (N_\sigma + 1) \times (N_\mu + 1)$ for the entries of the vector $\mathbf{f}^{(N_\sigma, N_\mu)}$. We solve this system by means of a Newton-Raphson scheme, which uses the iterative "bi-conjugate gradient stabilized method" [26] for inverting the Jacobian. This method works well only if an appropriate preconditioner is supplied. Here we utilize a finite difference representation of the Jacobian and invert it with the help of a band diagonal matrix decomposition algorithm (see, e.g., [27] and references therein). An initial guess for the Newton-Raphson scheme is taken from the unperturbed solution, $\{\phi_{\rm Kerr} \equiv 2\sqrt{M},\ V^i_{\rm Kerr} \equiv 0\}$ for which $\sigma_{\mathcal{H}} = \sigma_{\rm h}$. We depart gradually from this solution by modifying the location $\sigma_{\mathcal{H}}$ of the inner boundary in several steps. Any solution computed serves as the Newton-Raphson guess for the subsequent solution. In this way we can obtain large perturbations, as will be depicted in the next section.

TABLE I. Sample data for the construction of the initial data.

Calculation No.	j	$\sigma_{\rm h}$	$\sigma_{\mathcal{H}}$
1	0.5	1.0718	0.5
2	0.9	1.39286	1.4
3	0.999	1.91441	1.9145

VI. RESULTS

For any prescribed rotation parameter j with $0 \leq |j| < 1$, the numerical scheme permits the construction of initial data describing perturbations of the corresponding Kerr black hole. The deviation is tuned through

[7] As our perturbations lead to equatorially symmetric solutions, the restricted interval $\mu \in [0, 1]$ would suffice. However, we have chosen to keep the full interval to allow for non-equatorially symmetric perturbations that might become relevant in the future.

the prescription of the location $\sigma_{\mathcal{H}}$ of the inner boundary. Values of sample data are given in Table I:

We observe that the sign of the deviation from the unperturbed solution depends on the sign of $(\sigma_{\mathcal{H}} - \sigma_{\rm h})$, i.e., the location of the inner boundary with respect to the unperturbed solution.

In all calculations we find a rapid exponential decay of the Chebyshev coefficients of our numerical solution up to machine precision. Moreover, we see an exponential convergence rate with respect to the numerical resolution $(n_\sigma, n_\mu) = (N_\sigma + 1, N_\mu + 1)$. In particular, we monitor the quantities

$$D^{\phi}_{n_\sigma,n_\mu} = M^{-1/2} \sup_{\sigma,\mu} |\phi_{n_\sigma,n_\mu} - \phi_{60,30}| \qquad (50)$$

$$D^{i}_{n_\sigma,n_\mu} = M^{-2} \sup_{\sigma,\mu} |V^i_{n_\sigma,n_\mu} - V^i_{60,30}| \qquad (51)$$

which describe the maximal deviation from the numerical reference solution with $(n_\sigma, n_\mu) = (60, 30)$. For approximating the supremum, we take coordinate values $\sigma \in [0, \sigma_{\mathcal{H}}]$, $\mu \in [-1, 1]$ located on an equidistant grid of 500 times 500 points. For the examples listed in the table, we provide in figure 1 logarithmic plots displaying the deviations $\{D^{\phi}_{n_\sigma,n_\mu}, D^{i}_{n_\sigma,n_\mu}\}$. The exponential decay up to round-off error is a strong indication of the regularity of the solutions, i.e., for the regularity criterion (35). An occurrence of logarithmic terms would have become apparent by a mere power law decay.

Note that the perturbation for calculation No. 1 is large, as $r_{\mathcal{H}} = 2M/\sigma_{\mathcal{H}} \approx 2.14\, r_{\rm h}$. The corresponding potentials (ϕ, V^1, V^2, V^3) are displayed in figure 2. In contrast, the perturbations are small for the examples Nos. 2 and 3. In general, we can assure that our inner boundary is an apparent horizon if we choose the perturbation to be small enough. However, for large perturbations the outermost marginally trapped surface may be located further out. To clarify this point, we plan to apply a numerical apparent horizon finder in a future project. In this paper we stress the fact that we are able to construct arbitrarily small perturbations, even in a tiny vicinity of extreme Kerr black holes (see calculation No. 3). Note that we are not limited by some critical value $j_{\rm crit}$ below the extreme case[8].

A careful subsequent analysis of our solutions shows that the data constructed indeed correspond to *perturbed* Kerr black holes. In order to verify this point, we compute at the inner boundary mass and angular multipole moments M_n and J_n, which were introduced for isolated horizons by Ashtekar et al. [29]. We compare the moments with a reference Kerr solution possessing the same values for M_0 and J_1 and find that all higher moments are different from the corresponding Kerr expressions. In this manner we can conclude that our solutions do not represent the unperturbed Kerr solution in some new coordinates but do indeed describe *perturbed* Kerr data. An extensive description of this test is given in appendix VIII C.

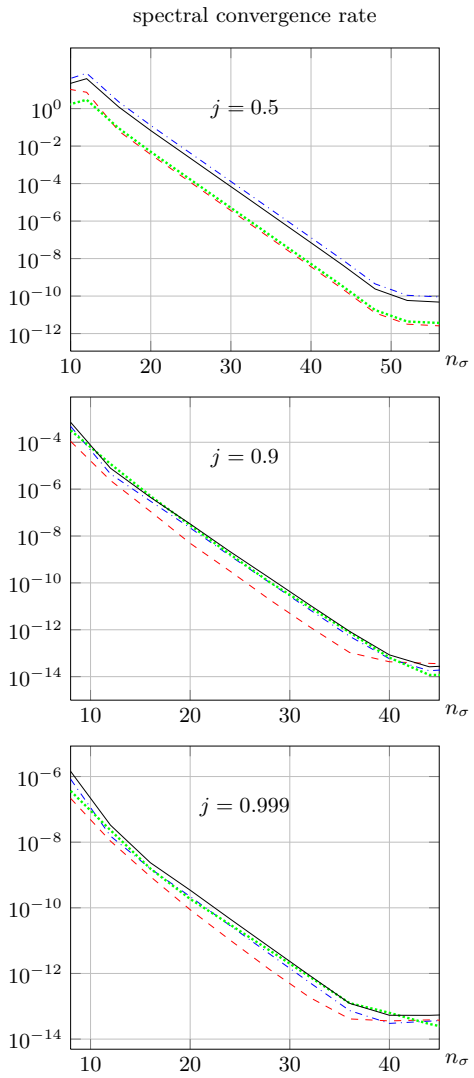

FIG. 1. For the examples listed in (I), the maximal deviations $D^{\phi}_{n_\sigma,n_\mu}$ (red, dashed), $D^{1}_{n_\sigma,n_\mu}$ (blue, dot-dashed), $D^{2}_{n_\sigma,n_\mu}$ (green, dotted) and $D^{3}_{n_\sigma,n_\mu}$ (black, solid) are displayed, see eqns. (50, 51). The numerical solutions have been calculated with the resolutions $(n_\sigma, n_\mu) = (n_\sigma, \frac{1}{2}n_\sigma)$.

VII. DISCUSSION

In this paper we have constructed single black hole initial data on compactified hyperboloidal slices on which the mean extrinsic curvature K approaches a constant asymptotically (ACMC-condition, $K = K_0 + K_4\sigma^4$). In particular, we were able to identify ACMC-slices for the Kerr solution and generated perturbed Kerr data

[8] In the case of conformally flat initial data, such a critical value $j_{\rm crit}$ has been observed, see e.g., [28] where $j_{\rm crit} \approx 0.97$.

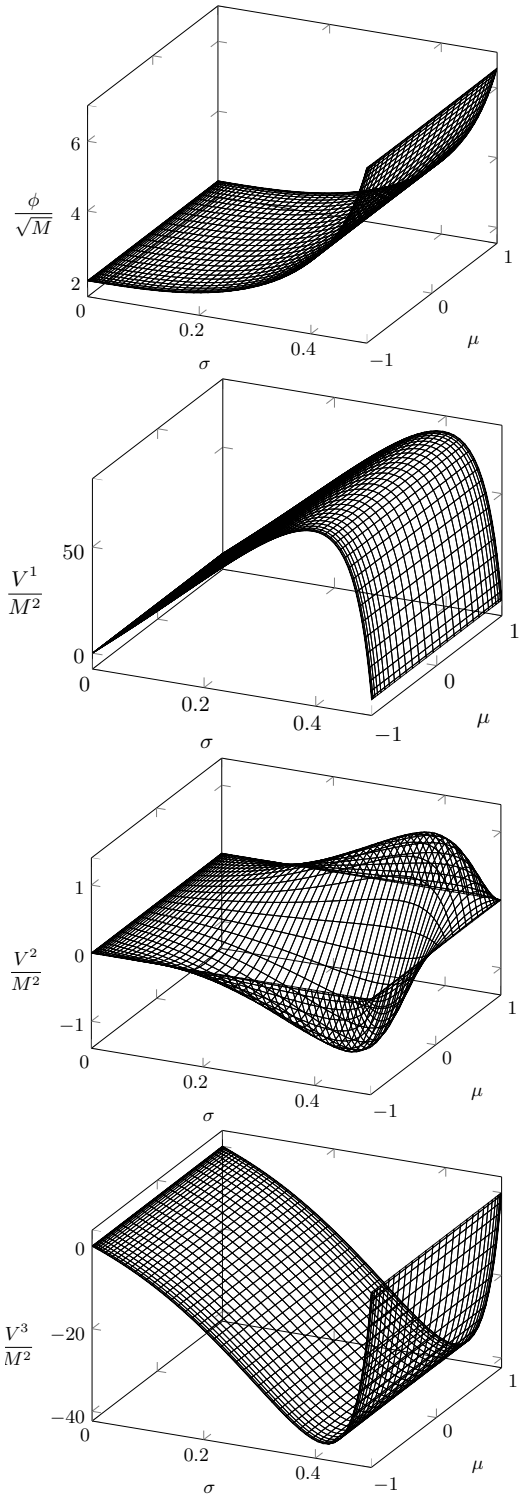

FIG. 2. The potentials $\{\phi, V^i\}$ for strongly perturbed Kerr initial data are displayed, see example No. 1 in (I). The rotation parameter is $j = 0.5$, and the inner boundary is located at $\sigma_{\mathcal{H}} = 0.5$ which corresponds to $r_{\mathcal{H}} \approx 2.14\, r_{\rm h}$.

from these. We find rapid exponential convergence of our pseudo-spectral solutions indicating the regularity of the potentials. Therefore, we believe that the stronger global CMC-condition, i.e., $K_4 \equiv 0$, which is adopted by several authors, can be replaced in favour of the local ACMC-condition without losing regularity. Note that the freedom provided by the ACMC-condition can be used to optimize the numerical representation. In this regard, a comparison of CMC- and ACMC-slices of the Schwarzschild metric is given in Appendix VIII B, showing that the CMC-condition needs more coefficients for an accurate spectral approximation.

The numerical solutions calculated in this work are meant to serve as initial data for a time-evolution code that solves the dynamical Einstein equations. For the development of such a code, we plan to realize the concept suggested by Zenginoğlu [30], i.e., we will treat the hyperboloidal evolution problem of the Einstein equations in terms of a conformally rescaled metric. Note that in Zenginoğlu's approach, the *wave gauge* is being utilized so that the Einstein equations become a system of wave equations. By taking as a starting point initial data corresponding to slightly perturbed Kerr black holes, we can explore the new code in the weakly non-linear regime where the equations should be similar to corresponding linearised ones. Numerical methods to realize this project are under construction.

ACKNOWLEDGEMENTS

It is a pleasure to thank L. Buchman, J. L. Jaramillo and A. Zenginoğlu for many valuable discussions and N. Johnson-McDaniel for carefully reading the manuscript. This work was supported by the DFG-grant SFB/Transregio 7 "Gravitational Wave Astronomy".

VIII. APPENDIX

A. The coordinate transformation leading to ACMC-slices

In section II we described the coordinate transformation (4, 5) which leads, for the Kerr solution, from Kerr coordinates to compactified hyperboloidal slices on which the ACMC-condition (8) is valid. The equations (4, 5) contain an auxiliary function $A = A(\sigma, \mu)$ which was determined through an appropriate diagonal Padé expansion. Here we provide the explicit form of this function:

$$A(\sigma, \mu) = \frac{\sigma Z}{N}$$

with

$$\begin{aligned} Z &= 24c_1\left(c_1c_3 - c_2^2\right) - \left(a_4c_1^2 + 24c_2^3 - 48c_1c_2c_3\right)\sigma \\ N &= 24\left(c_1c_3 - c_2^2\right) + (24c_2c_3 - a_4c_1)\sigma \\ &\quad + \left(a_4c_2 - 24c_3^2\right)\sigma^2. \end{aligned}$$

The coefficients $c_i = c_i(\mu\,; j)$ are given by:

$$\begin{aligned} c_1 &= a_1 - \frac{j^2\mu^2}{16} \\ c_2 &= \frac{1}{8}\left(j^2-4\right) \\ c_3 &= -\frac{1}{6}\left(8+12a_1+6a_1^2-j^2\right) + \frac{1}{8}(1+a_1)j^2\mu^2 \\ &\quad -\frac{j^4\mu^4}{256}. \end{aligned}$$

To fix the free parameters a_1 and a_4 as functions of j, we analyse the decay of the Chebyshev coefficients $c_k^{(\tilde\alpha)}$ of the conformal lapse $\tilde\alpha$ (see section II and footnote 3 therein). We fit their logarithm linearly over the index, i.e.

$$\text{Fit}\left[\log(M|c_k^{(\tilde\alpha)}|)\right] = f_1 + f_2\cdot k.$$

and perform a numerical minimization of f_2 with respect to a_1 and a_4 using a simplex algorithm. In this way we obtain the parameters corresponding to the most rapid decay. We observe that the results obtained in this manner are well represented by a simple quadratic fit,

$$\begin{aligned} a_1 &= \frac{113}{100} + \frac{9}{500}|j| + \frac{3}{40}j^2 \\ a_4 &= 4!\left(\frac{161}{10} + \frac{3}{4}|j| - \frac{5}{2}j^2\right). \end{aligned}$$

Note the occurrence of terms containing $|j|$ which is a result of the specific quadratic fit we have chosen. In a more fundamental treatment one would try to avoid such terms, as the Kerr solution should be described by metric coefficients that are smooth with respect to j. However, for the purpose of this paper it is convenient to utilize the above choice, as it realizes with little effort ACMC-slices possessing smooth functions $\tilde\alpha$ with rapidly decaying Chebyshev coefficients.

B. Comparison of ACMC- with CMC-slices

In this section we perform a numerical comparison of our ACMC-slices with CMC-slices in the case of the spherically symmetric Schwarzschild black hole. The comparison consists again of analyzing the decay of the Chebyshev coefficients $c_k^{(\tilde\alpha)}$ of the conformal lapse $\tilde\alpha$ in the two situations.

For the Schwarzschild metric we have $j = 0$, and the corresponding auxiliary function A, appearing in the coordinate transformation leading to ACMC-slices, becomes independent of μ,

$$A(\sigma)_{\text{ACMC}} = \frac{3(4478917900\sigma^2 + 1950390283\sigma)}{5178027300 + 14182095000\sigma + 28592255449\sigma^2}.$$

A plot of this function is provided in figure 3. Also, the corresponding mean curvature K_{ACMC} is displayed therein. Note that the asymptotic value of the mean curvature is [see equations (17) and (20)]

$$K_{0,\text{ACMC}} = \frac{3}{4M\sqrt{1+a_1}} = \frac{5}{2M}\sqrt{\frac{3}{71}} \approx 0.514M^{-1}.$$

With the conformal factor $\Omega = \sigma/4M$, the associated conformal lapse turns out to be

$$\tilde\alpha_{\text{ACMC}} = \frac{2}{M\sqrt{(\sigma-1)\sigma^2A'(\sigma)^2 + (1-2\sigma^2)\,A'(\sigma) + \sigma + 1}}.$$

In figure 4, the decay of the coefficients $M\,c_k^{(\tilde\alpha_{\text{ACMC}})}$ is displayed.

We now turn our attention to CMC-slices. In the Schwarzschild case, the line element (1) reduces to the Eddington-Finkelstein form, describing ingoing null rays. As described in [31–33], the coordinate transformation between the coordinates $(V, r, \vartheta, \varphi)$ and coordinates $(T, r, \vartheta, \varphi)$, in which the slices $T =$ constant satisfy the CMC-condition, is given by

$$T = V - \int \frac{rdr}{r-2M} - \int \frac{radr}{(r-2M)f},$$

where

$$f = \sqrt{1 - \frac{2M}{r} + a^2}, \qquad a = \frac{Kr}{3} - \frac{C}{r^2} \tag{52}$$

and K is the constant mean curvature. The parameter C represents an additional one-parameter degree of freedom in the choice of spherically symmetric CMC-slices in the Schwarzschild metric. For slices extending up to $\mathscr{I}^+$ we have

$$C > \frac{8}{3}KM^3,$$

hence $a|_{r=2M} = -f|_{r=2M} < 0$. From the relation between T and V, we can read off the transformation leading from Eddington-Finkelstein-slices to compactified CMC-slices. Putting $T = 4M\tau$, we obtain

$$\begin{aligned} r &= \frac{2M}{\sigma} \\ V &= 4M\left(\tau + \frac{1}{\sigma} - \log(\sigma) + A_{\text{CMC}}(\sigma)\right) \end{aligned}$$

with the function A_{CMC} given by:

$$A_{\text{CMC}} = \int \frac{f+a}{2\sigma^2(\sigma-1)f}d\sigma + \log(\sigma) - \frac{1}{\sigma}$$

Note that despite the apparently singular form, A_{CMC} is *analytic* on the entire interval $\sigma \in [0,1]$.

Using again the conformal factor $\Omega = \sigma/4M$, the associated conformal lapse reads

$$\tilde\alpha_{\text{CMC}} = \frac{1}{48M}\sqrt{144(1-\sigma)\sigma^2 + (8KM - 3CM^{-2}\sigma^3)^2}.$$

Now, utilizing a method similar to the one described in section VIII A, we find that strong decay rates of the corresponding coefficients $c_k^{(\tilde{\alpha}_{\rm CMC})}$ are realised if we put the free parameters as

$$K \approx 0.32M^{-1}, \qquad C \approx 2.88M^2.$$

In figure 3, the quantities $\{A_{\rm ACMC}, A_{\rm CMC}\}$ as well as the corresponding mean curvatures $\{K_{\rm ACMC}, K_{\rm CMC}\}$, obtained for these settings, are plotted.

Figure 4 shows the convergence of the Chebyshev coefficients $\{M\, c_k^{(\tilde{\alpha}_{\rm ACMC})}, M\, c_k^{(\tilde{\alpha}_{\rm CMC})}\}$. While the coefficients $|M\, c_k^{(\tilde{\alpha}_{\rm ACMC})}|$ for the ACMC-slice reach 10^{-16}, i.e. the order of machine precision ($\sim$ 16 digits), at $k = 32$, the coefficient $|M\, c_{32}^{(\tilde{\alpha}_{\rm CMC})}|$ for the CMC-slice is only about 10^{-12}, i.e. larger by 4 orders of magnitude. We thus conclude that the replacement of the global CMC-condition in favour of the local ACMC-condition provides advantages in a numerical treatment.

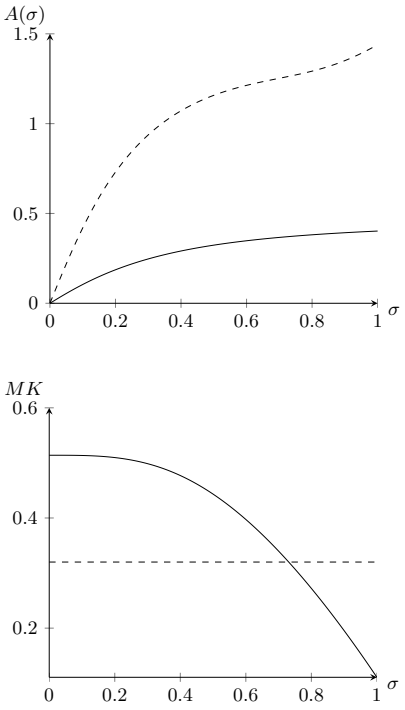

FIG. 3. The quantities $A = A(\sigma)$ and $MK = MK(\sigma)$ for CMC-slices (dashed) and ACMC-slices (solid) case are plotted in the Schwarzschild case $j = 0$. The slices possess asymptotic mean curvature values at $\mathscr{I}^+$ of $K_0 \approx 0.514M^{-1}$ for the ACMC-slicing and $K_0 \approx 0.32M^{-1}$ for the CMC-slicing. The additional parameter C in the family of CMC-slices has been set to $CM^{-2} \approx 2.88$.

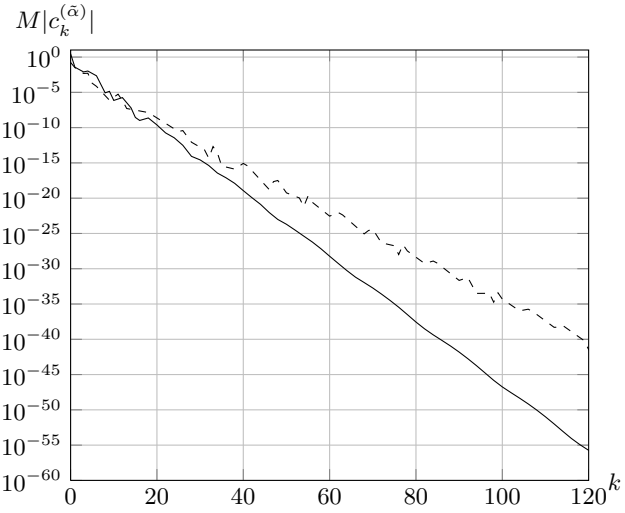

FIG. 4. Chebyshev coefficients of the conformal lapse $\tilde{\alpha}$ for the Schwarzschild metric in CMC-coordinates (dashed) and ACMC-coordinates (solid). For the ACMC-slice, the order of machine precision, that is 10^{-16}, is reached at $k = 32$, while for the CMC-slice the corresponding coefficient is of the order 10^{-12}.

C. Mass and Angular Multipole Moments

Having obtained the numerical solution of the constraint equations, we perform a source multipolar decomposition of the marginally outer-trapped surface $\mathcal{H}$ characterizing the inner boundary of our numerical domain. Although we focus here on small perturbations around the Kerr solution, we note that the expansion scalar of outgoing null rays on surfaces inside the numerical domain ($\sigma < \sigma_{\mathcal{H}}$) is positive even for the stronger perturbation depicted in Fig. (2). This result is significant evidence that, also in these cases, we are still dealing with apparent horizons, i.e. *outermost* marginally outer-trapped surfaces.

Introduced in [29], the multipole moments of isolated horizons are an invariant measure on $\mathcal{H}$ that allow us to tell if the new initial data represents, indeed, a deformed black hole or if it is rather just a new slice of the Kerr space-time (with possibly new parameters M and j) [34]. In fact, as was shown in [29], the geometry of a given isolated horizon as well as its vicinity are completely characterized by multipole modes divided into two types: mass modes M_n and angular modes J_n. In the case of dynamical horizons, they were first employed in [35], where the authors, among other results, used them to verify that during the numerical evolution of a space-time, the black hole settles down to a Kerr solution.

In order to define the horizon's angular momentum in a gauge-independent manner, the calculation of such multipoles relies on the existence of a preferred divergence-free vector field Φ^a on $\mathcal{H}$, which here is taken to be the axial Killing vector ∂_φ. Another important issue for their construction is the introduction of a new coordinate system $\{\hat{\mu}, \hat{\varphi}\}$ on $\mathcal{H}$, in such a way that the Legendre polynomials $P_n(\hat{\mu})$ hold the correct orthonormality properties. As described in [29, 35], $\hat{\varphi} \in [0, 2\pi)$ is the affine-parameter along Φ^a which coincides, in our case, with the original

coordinate φ. Apart from that, $\hat{\mu} = \cos\hat{\theta} \in [-1, 1]$ is defined by

$$\partial_a \hat{\mu} = \frac{1}{R_{\mathcal{H}}^2} {}^{(2)}\epsilon_{ba} \Phi^b, \tag{53}$$

with ${}^{(2)}\epsilon_{ba}$ the area-element form on $\mathcal{H}$ and $R_{\mathcal{H}}$ the areal radius defined by the area of $\mathcal{H}$, i.e., $A_{\mathcal{H}} = \oint_{\mathcal{H}} dA = 4\pi R_{\mathcal{H}}^2$. The integration constant in (53) is determined by requiring $\oint_{\mathcal{H}} \hat{\mu} dA = 0$.

The angular and mass multipoles are then defined as

$$J_n = \frac{R_{\mathcal{H}}^{n-1}}{8\pi} \oint_{\mathcal{H}} K_{\Phi s}(\mu) P_n'\left(\hat{\mu}(\mu)\right) dA \tag{54}$$

$$M_n = M_{\mathcal{H}} \frac{R_{\mathcal{H}}^n}{8\pi} \oint_{\mathcal{H}} {}^{(2)}R(\mu) P_n(\hat{\mu}(\mu)) dA. \tag{55}$$

In Eq. (54), $K_{\Phi s} = K_{ij}\Phi^i s^j$ and the derivative of P_n should be taken with respect to its argument $\hat{\mu}$. Apart from that, in Eq. (55), ${}^{(2)}R$ is the Ricci scalar of the two-surface $\mathcal{H}$ and the parameter $M_{\mathcal{H}}$ is given by $M_{\mathcal{H}} = \sqrt{R_{\mathcal{H}}^2/4 + J_1^2/R_{\mathcal{H}}^2}$, which corresponds to black-hole mass in case of the Kerr space-time.

Using the Gauss-Bonnet theorem, it is not hard to convince oneself that $M_0 = M_{\mathcal{H}}$. One can also show that $M_1 = 0$ [29, 36]. Regarding the angular modes, J_0 is clearly zero and J_1 is exactly the definition of the Komar angular momentum on the horizon. Finally, due to the symmetry across the equatorial plane presented by our initial data, all the odd M_n as well as the even J_n vanish.

Given the numerical initial data, calculated as described in the previous sections, we evaluate the multipole modes (54) and (55) with respect to the coordinate sphere $\sigma_{\mathcal{H}}$. If our solution were just a new slice of a Kerr space-time, the corresponding mass and angular momentum parameters of the metric would be given, respectively, by M_0 and J_1. In this way, the comparison of higher modes allows us to distinguish a perturbed black hole from the Kerr solution.

It is worth to mention that both multipoles modes, as defined in eqns. (54) and (55), have physical dimensions of $[\text{Mass}]^{n+1}$. However, as we do not want to attach any strong physical meaning to the multipoles, but rather just use them as an unambiguous tool to discriminate our initial data form the Kerr solution, we present our results in terms of the normalized modes J_n/M_0^{n+1} and M_n/M_0^{n+1}.

Fig. 5 depicts results for small perturbations around the Kerr solution. In particular, the top, middle and bottom panel have the parameter $j = 0.5$, $j = 0.9$ and $j = 0.999$, respectively. The corresponding horizon were deformed to $\sigma_{\mathcal{H}} = 1.07$, $\sigma_{\mathcal{H}} = 1.4$ and $\sigma_{\mathcal{H}} = 1.9145$ (their original values are given in Table I). We find that the multipole modes confirm our expectation that the new initial data represent deformed and rotating black holes. In fact, the inset within each panel shows that the multipole modes of our perturbed initial data do not agree with the ones corresponding to the Kerr solution with the same parameters M_0 and J_1 .

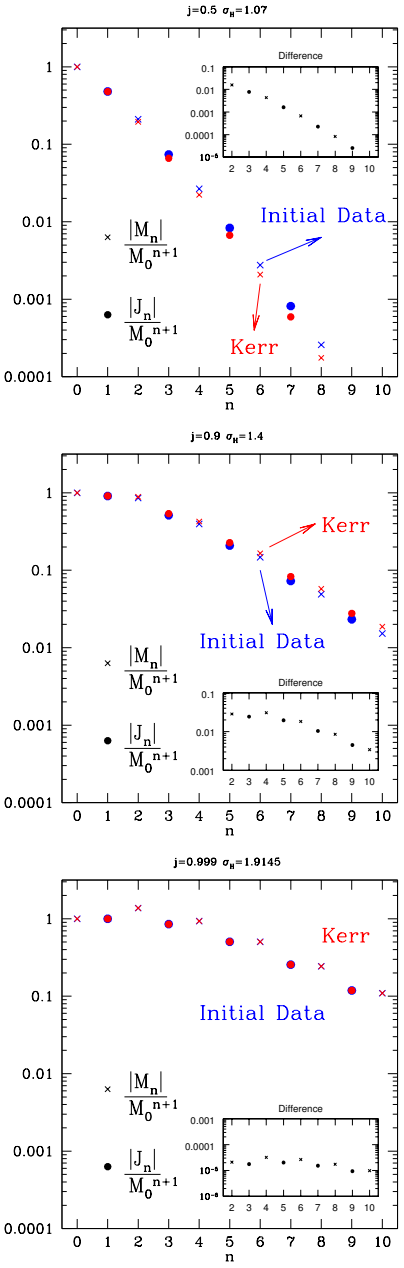

FIG. 5. The top, middle and bottom panel show, respectively, the multipole modes for solutions obtained with $j = 0.5$, $j = 0.9$, and $j = 0.999$ and inner boundary set, respectively, to $\sigma_{\mathcal{H}} = 1.07$, $\sigma_{\mathcal{H}} = 1.4$, $\sigma_{\mathcal{H}} = 1.9145$ (original values are given in Table I). The non-agreement between them confirms that our initial data do not correspond to a different slice of the Kerr solution. Crosses and dots correspond, respectively, to the regularized mass $|M_n|/M_0^{n+1}$ and the angular $|J_n|/M_0^{n+1}$ modes, while the inset shows the difference between their values for the perturbed black hole and the corresponding Kerr solution with the same M_0 and J_1 parameters.

[1] J. Frauendiener, Living Reviews in Relativity **7** (2004).
[2] H. Bondi, M. van der Burg, and A. Metzner, Proc.Roy.Soc.Lond. **A269**, 21 (1962).
[3] J. Stewart, Proc. R. Soc. London, Ser. A **424**, 211 (1989).
[4] H. Friedrich, Communications in Mathematical Physics **91**, 445 (1983).
[5] P. Hübner, Class.Quant.Grav. **18**, 1871 (2001).
[6] V. Moncrief and O. Rinne, Classical and Quantum Gravity **26**, 125010 (2009).
[7] O. Rinne, Class.Quant.Grav. **27**, 035014 (2010).
[8] J. Frauendiener, Journal of Computational and Applied Mathematics **109**, 475 (1998).
[9] L. T. Buchman, H. P. Pfeiffer, and J. M. Bardeen, Phys.Rev. **D80**, 084024 (2009).
[10] J. M. Bowen and J. York, James W., Phys.Rev. **D21**, 2047 (1980).
[11] L. Andersson, P. T. Chruściel, and H. Friedrich, Commun.Math.Phys. **149**, 587 (1992).
[12] L. Andersson and P. T. Chruściel, Phys. Rev. Lett. **70**, 2829 (1993).
[13] L. Andersson and P. T. Chruściel, Communications in Mathematical Physics **161**, 533 (1994).
[14] J. W. York, Jr., in *Sources of Gravitational Radiation*, edited by L. L. Smarr (1979) pp. 83–126.
[15] J. W. York, Jr. and T. Piran, in *Spacetime and Geometry*, edited by R. A. Matzner and L. C. Shepley (1982) p. 147.
[16] A. Zenginoğlu, Class.Quant.Grav. **25**, 145002 (2008).
[17] R. M. Wald, *General Relativity* (University of Chicago Press, 1984).
[18] C. Misner, K. Thorne, and J. Wheeler, *Gravitation* (W.H. Freeman, San Francisco, 1973).
[19] J. M. Bardeen and L. T. Buchman, Phys.Rev. **D85**, 064035 (2012).
[20] J. W. York, Jr., in *Frontiers in Numerical Relativity*, edited by C. Evans, L. Finn, and D. Hobill (Cambridge University Press, 1989) pp. 89–109.
[21] M. F. Huq, M. W. Choptuik, and R. A. Matzner, Phys. Rev. D **66**, 084024 (2002).
[22] L. Andersson and J. Metzger, Commun.Math.Phys. **290**, 941 (2009).
[23] L. Andersson, M. Mars, J. Metzger, and W. Simon, Class.Quant.Grav. **26**, 085018 (2009).
[24] T. Chu, H. P. Pfeiffer, and M. I. Cohen, Phys.Rev. **D83**, 104018 (2011).
[25] R. Meinel, M. Ansorg, A. Kleinwächter, G. Neugebauer, and D. Petroff, *Relativistic Figures of Equilibrium* (Cambridge University Press, 2008).
[26] R. Barrett, M. Berry, T. F. Chan, J. Demmel, J. Donato, J. Dongarra, V. Eijkhout, R. Pozo, C. Romine, and H. V. Vorst, *Templates for the Solution of Linear Systems: Building Blocks for Iterative Methods, 2nd Edition* (SIAM, Philadelphia, PA, 1994).
[27] W. H. Press, S. A. Teukolsky, W. T. Vetterling, and B. P. Flannery, *Numerical Recipes 3rd Edition: The Art of Scientific Computing*, 3rd ed. (Cambridge University Press, New York, NY, USA, 2007).
[28] G. Lovelace, R. Owen, H. P. Pfeiffer, and T. Chu, Phys. Rev. D **78**, 084017 (2008).
[29] A. Ashtekar, J. Engle, T. Pawlowski, and C. Van Den Broeck, Class. Quant. Grav. **21**, 2549 (2004).
[30] A. Zenginoğlu, Class.Quant.Grav. **25**, 195025 (2008).
[31] D. R. Brill, J. M. Cavallo, and J. A. Isenberg, Journal of Mathematical Physics **21**, 2789 (1980).
[32] E. Malec and N. Ó Murchadha, Phys. Rev. D **68**, 124019 (2003).
[33] E. Malec and N. Ó Murchadha, Phys. Rev. D **80**, 024017 (2009).
[34] N. Vasset, J. Novak, and J. L. Jaramillo, Phys.Rev. **D79**, 124010 (2009).
[35] E. Schnetter, B. Krishnan, and F. Beyer, Phys. Rev. D **74**, 024028 (2006).
[36] J. L. Jaramillo, R. P. Macedo, P. Moesta, and L. Rezzolla, Phys. Rev. D **85**, 084030 (2012).